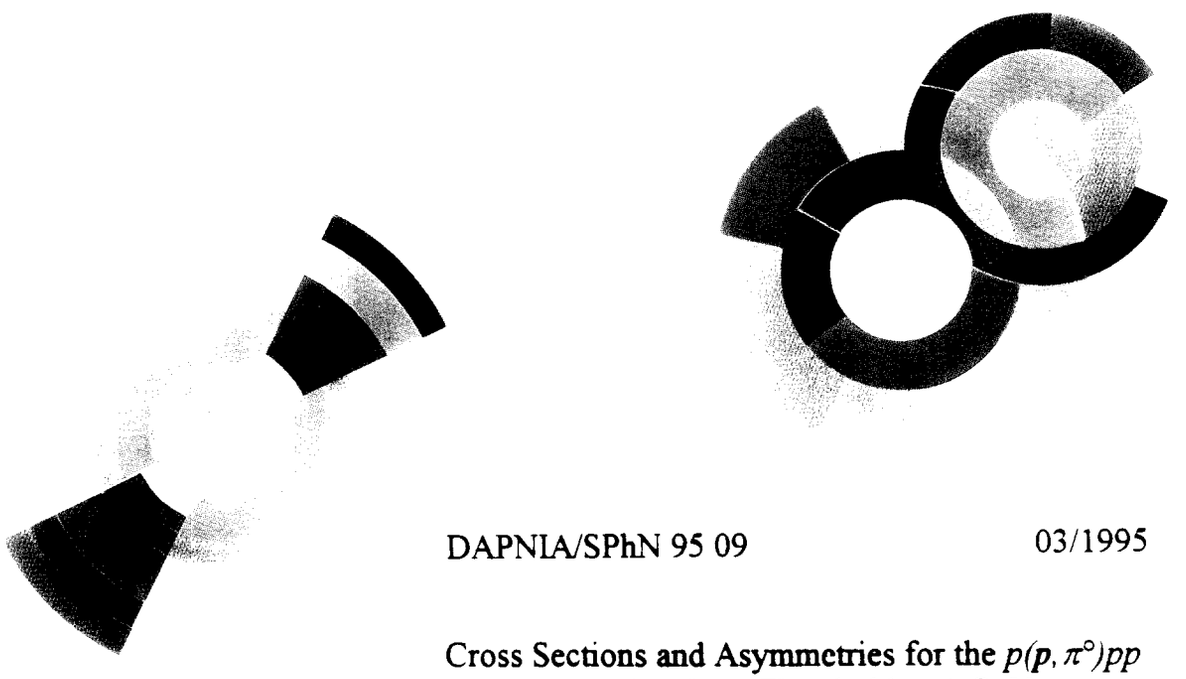

DAPNIA/SPhN 95 09 03/1995

Cross Sections and Asymmetries for the $p(\vec{p}, \pi^\circ)pp$ Reaction from Threshold to 1 GeV

G. Rappenecker, M. Rigney, J.P. Didelez, E. Hourani,
L. Rosier, J. van de Wiele, G. Berrier-Ronsin, A. Elayi,
R. Frascaria, P. Hoffman-Rothe,
G. Anton, J. Arends, M. Breuer, K. Büchler, G. Noldeke,
B. Zucht,
G. Blanpied, B. Preedom,.
J.M. Laget, B. Saghaï

DAPNIA

Le DAPNIA (**D**épartement d'**A**strophysique, de physique des **P**articules, de physique **N**ucléaire et de l'**I**nstrumentation **A**ssociée) regroupe les activités du Service d'Astrophysique (SAp), du Département de Physique des Particules Elémentaires (DPhPE) et du Département de Physique Nucléaire (DPhN).

Adresse : DAPNIA, Bâtiment 141
CEA Saclay
F - 91191 Gif-sur-Yvette Cedex

A paraître dans Nuclear Physics A

Cross Sections and Asymmetries for the $p(\vec{p},\pi^\circ)pp$ Reaction from Threshold to 1 GeV.

G. Rappenecker[2], M. Rigney, J.P. Didelez, E. Hourani, L. Rosier, J. van de Wiele, G. Berrier-Ronsin, A. Elayi, R. Frascaria, P. Hoffmann-Rothe,

IN2P3, Institut de Physique Nucléaire, 91406 Orsay, France

G. Anton, J. Arends[1], M. Breuer, K. Büchler[2], G. Nöldeke, B. Zucht[3],

Physikalisches Institut der Universität Bonn, Germany

G. Blanpied, B. Preedom,

University of South Carolina, 29208 Columbia, USA

J.M. Laget, B. Saghai

Laboratoire DAPNIA/SPN, 91191 Gif-sur-Yvette, France

Abstract: Total cross sections, differential cross sections, and asymmetries for the reaction $p(\vec{p},\pi^\circ)pp$ from threshold to 1 GeV have been measured. The outgoing π° was detected by a 4π neutral meson spectrometer. Our data are compared with the corresponding $np \to NN\pi^\pm$ reactions. The isoscalar partial cross sections are extracted from the relevant total cross sections. They are significant throughout the whole energy range. Below the Δ region, energy integrated differential cross sections show a large anisotropy difference between the neutral and charged pion channels respectively. A partial wave fit shows that the initial $T=0$ state is dominated by the $^3D_1$ wave in this energy region. Finally, predictions of phenomenological models give reasonable good account of the measured observables but cannot reproduce the sign of the asymmetries.

E | NUCLEAR REACTION $^1H(\vec{p},\pi^\circ)$, 325MeV < E_p < 1012MeV,
measured: σ, $d\sigma/d\Omega$, A_y,
deduced: partial σ, partial waves.

[2]Now with the Asea Brown Boveri, KWL GmbH, Mannheim, Germany
[1]Now with the Institut für Kernphysik der Universität Mainz, Mainz, Germany
[2]Now with Elekluft, Bonn, Germany
[3]Now with MS Mikro Software, Bad Münstereifel, Germany
*Supported in part by the CEE "Human Capital and Mobility" and the National Science Foundation.

1. Introduction

Nucleon-nucleon (NN) scattering with single pion production has been studied for more than forty years now, and the experimental and theoretical results have been reviewed several times [1-3]). This class of reactions can be described by only four independent partial cross sections σ_{if}, the indices are related to the two nucleon's isospin in initial and final state [4,5]) which can only be 0 or 1. A major interest for the reaction

$$pp \rightarrow pp\pi^{\circ} \tag{1.1}$$

is the fact that it is the only one in this class with a pure σ_{11} cross section, whereas in all other single pion production reactions, except those with a deuteron in the final state, at least two partial cross sections contribute. In particular, the reactions

$$np \rightarrow NN\pi^{\pm} \tag{1.2}$$

are related to σ_{11} and σ_{01} by

$$\sigma_{(np\rightarrow NN\pi^{\pm})} = \frac{1}{2}(\sigma_{01} + \sigma_{11}), \tag{1.3}$$

therefore

$$\sigma_{01} = 2\sigma_{(np\rightarrow NN\pi^{\pm})} - \sigma_{(pp\rightarrow pp\pi^{\circ})}. \tag{1.4}$$

As described in a previous paper [6]), we have measured accurately total cross sections corresponding to reaction (1.1), in order to derive σ_{01} by comparison to reaction (1.2) between 480 and 560 MeV and have shown that σ_{01} is significantly different from zero in this energy range. We pointed out, however, the lack of precise enough experimental results, in particular for absolute values, both on neutral pion [7-17]) and charged pion [18-25]) production. Since the rise of σ_{01} with energy provides a powerful tool to determine it, provided reactions (1.1) and (1.2) are measured on a wide energy range, we report in this paper measurements of total cross sections for reaction (1.1), from threshold to 1 GeV.

Differences in the angular dependence of the pion energy integrated cross sections for reaction (1.1) and (1.2) can also be ascribed to σ_{01}. The 4π configuration of our new neutral meson spectrometer SPES02π permitted the measurement of the π° angular dependence, with a much better precision than has been done previously. Below the Δ region around 540 MeV, we confirm the substantial difference between anisotropy parameters corresponding to reactions (1.1) and (1.2) respectively, which leads to a non-negligible σ_{01} contribution of pronounced anisotropy. In particular, a partial wave fit shows that the σ_{01} is completely dominated by the $^3D_1$ wave which has a resonant behavior around 540 MeV. Finally, beam asymmetries have been measured throughout the whole energy range. They are negative and comparable to those corresponding to reaction (1.2), however, present phenomenological models cannot give good account of the asymmetry sign. The

new experimental results reported here benefit from recent and precise data for the charged pion channels, both concerning the angular distributions [26]) and the asymmetries [27,28]), published since our previous paper. In this paper, section 2 is devoted to the description of the experimental set-up, section 3 describes the data analysis, a discussion of the experimental results, with comparison to theoretical predictions is given in section 4 and the conclusions in section 5.

2. The Experimental Setup

2.1. THE SPES0-2π

The fig. 1 shows a schematic view of the detector arrangement called SPES02π. The principle of operation of the π° spectrometer SPES02π has been described in detail in [6]); however, the geometry has been modified to be of the 4π type, see Ref. 29 for complete details. The SPES02π consists essentially of 24 lead-glass bars (F2 type) [30]), arranged vertically in two cylindrical concentric shells of 8 and 16 bars respectively like two sides of a clam shell arround the target and the beam pipe. The bars serve as Čerenkov counters for the Čerenkov light produced by the leptons of the electromagnetic showers induced by the photons of the decaying pions. All bars are 8 cm thick, which corresponds to 2.4 radiation lengths and have a trapezoidal form to be arranged in a cylindrical shape without leaving any open space between them. In the first shell each bar is 69 cm in length and covers 30° in the horizontal angle, while in the second shell the bars are 116 cm in length and cover an angle of 15° each. By using longer bars for the second shell located farther away from the target center, the same solid angle is covered by both shells. Each bar is equipped with two photomultiplier tubes, type XP 2252 B [31]), one at each end. These 12 stage, 1 $\frac{7}{8}$ inch tubes, have been chosen because of their borosilicate window having better UV transmission, and high gain at the first dynode, thus permitting thresholds at the level of one single photoelectron (PE). The energy correspondence linking the number of PE produced at PM photocathodes to the energy of the gamma-ray was 1.85 PE/MeV. In front of each bar of the inner shell and covering it, there is a scintillator to tag charged particles of competing reactions. Those 8 scintillator slabs ($70 \times 5 \times 1$ cm^3), viewed at one end by a photomultiplier, were also cut with a trapezoidal cross section in order to completely cover the first shell lead-glass bars with as small as possible gap between them.

Located between the two shells of lead-glass bars and directly behind each of the first shell bars, are eight "Limited Streamer Tubes"(LST) [32]). These gas tubes, operating in the limited streamer mode, are sensitive to the leptons of the electromagnetic showers initiated in the first shell and allow the position determination of the γ-rays impact in the horizontal and vertical plane. These units cover about 25% of the detectors solid angle and have a detection efficiency of the order of 70%, thus only a little more than 10% of the registered events had both photons detected

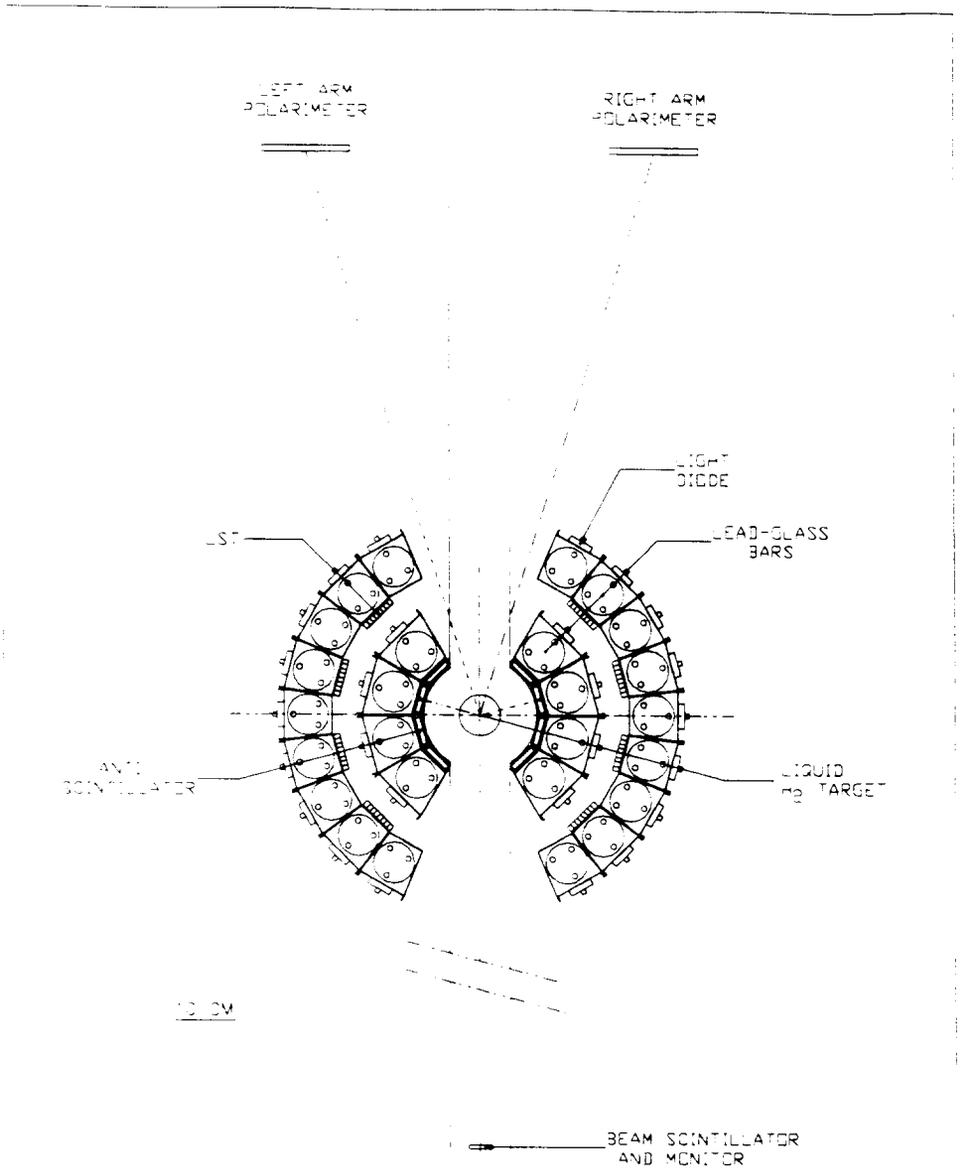

Fig. 1. Experimental setup of the SPES02π spectrometer and beam monitors (top view).

by the LST simultaneously. This small sample of events was used to calibrate the vertical and horizontal localization of the shower obtained, for all events, by the time difference of the light pulse arriving at the extremities of a lead-glass bar and by the granularity of the system.

The central hole of the detector was occupied by a cryostat containing the liquid hydrogen target, (507 mg/cm^2). The target cell was made of a 70 μm thick kapton foil, rolled in a cylindrical shape forming a container of 7 cm diameter and 8 cm height. The total window thickness seen by the beam was therefore only 16 mg/cm^2. In addition, the target cryostat shared the vacuum of the beam line, allowing the transport of the beam under vacuum until the beam stopper.

All photomultipliers of the inner shell bars were connected to constant fraction discriminators to eliminate the time walk induced by signals of various amplitudes. The corresponding outgoing logic signals of the two tubes of each bar were sent to logic meantimers delivering a time signal independent of the impact position along the bar and also to a Time-to-Digital Converter (TDC). Likewise, the logic signals coming from the beam scintillator were sent to a TDC. The analog sums of the two linear signals of the PM of each lead-glass bar were sent to Analog-to-Digital Converters (ADC). A pattern unit registered the type of event selected by the trigger, keeping track of the hits in the first shell bars and in the anticoïncidence counters to allow an offline control of the fast trigger selectivity. Scalers also counted free running and inhibited rates of the polarimeter coïncidences and the rate of the beam scintillator. All the data were read and written to hard disk using a data acquisition system based on the "Q" system from Los Alamos [34]) and later archived on 8 mm magnetic tapes.

A fast, topological trigger was installed using the programmable Memory Lookup Unit (MLU) from LeCroy [35]). A good event consisted of any number from 2 to 4 first shell lead-glass bars having a pattern compatible with a π^0 decay; namely two groups of bars (corresponding to the two gamma rays) without any hits in the anticoïncidence detectors in front (to disregard charged particles). The output of the MLU in response to the 16 inputs: the 8 lead-glass meantimers and the 8 anticoïncidence logical signals is available about 60 ns after the inputs. This output signal is then put in coïncidence with the beam scintillator to give the general trigger; the beam scintillator defining the timing. A strobe signal needed for the MLU is defined by a coïncidence between the beam scintillator and a logical OR of the 8 signals coming from the top of the 8 bars in the first shell.

2.2. BEAM MONITORING AND POLARIMETER

The SATURNE accelerator provides protons with a kinetic energy of up to 3 GeV, however, the beam line where the SPES02π had been installed can only accommodate protons up to 1.1 GeV. In our case, the time structure of the beam consisted of

bursts of about 0.3 seconds in length with a 1.3 second repetition rate. The beam intensity was limited to the order of $5 \cdot 10^5$ protons/burst by the number of events accepted by the trigger, compatible with the computer data acquisition rate ($\approx$ 100 triggers/sec). This low intensity allowed the use of a scintillator in the beam which provided both a time reference for each event and the absolute beam intensity, counting incident protons one by one. This "Beam Scintillator" having dimensions ($50 \times 50 \times 4$ mm^3) was installed 4 m upstream from the target. A standard ionization chamber, placed at the end of the beam line, provided a current proportional to the beam intensity which was integrated at the end of each burst to give a signal scaling the number of protons. Using those two independent measurements of the beam intensity, we could verify that counting losses in the beam scintillator due to pile-up occurred only above 10^6 protons/sec which was the case less than 5% of the time during the whole experiment. Furthermore, bursts of abnormal intensity could be eliminated from the data set.

The proton beam was polarized in a direction perpendicular to the reaction plane with the sequence of bursts: "zero, up, up, down, down". We used two different polarimeters to measure and monitor the degree of beam polarisation. The synchrotron SATURNE, being a strong focusing ring, the polarization must be measured after the extraction of the beam. For the absolute measurement the standard and well calibrated SATURNE polarimeter installed on another extraction line was used. It uses the elastic proton-proton data to measure the polarization from proton scattering on a CH_2-target. It consists of two scintillator telescopes (left and right) to measure the forward protons, and two counters under 90^o to catch the recoil protons. The angular positions are adjusted with beam energy and tuned to be at maximum analyzing power. There is an identical device in the vertical plane to calibrate the relative intensity of the different polarization states. This polarimeter has been calibrated, tested, and used many times [33]). The SPES02π also has its own polarimeter to monitor the polarization's stability during the experiment. It measures the proton-proton scattering asymmetry, using the liquid hydrogen target of the experiment. It consists of two scintillators one meter downstream from the target, forming the forward part of the left and right arms. Each of these counters is put in coïncidence with the relevant anticoïncidence counters of the inner shell to form the backward part of the left and right arms, making an opening angle of about 90^o between the two detected protons, see fig. 1. The mean angle of the forward proton was fixed at 18°, close enough to the optimal position at any incident proton energy, given the angular coverage of the forward scintillator of 10°. Large acceptance detectors were used to obtain high enough counting rates for a single burst of 10^5 protons/sec. This online polarimeter was used to disregard bursts with unstable polarization compared to the average value and contributed enormously to the quality of the data. It allowed the verification that the absolute degree of polarization was about 85% for all energies, except at 1012 MeV beam energy where

it dropped to 58% and was very stable during the measurements.

3. Data Analysis and Results

3.1. DATA REDUCTION

Before the detailed analysis was undertaken, a systematic study of all the beam monitoring was performed for each run on a burst-by-burst basis. This included: monitoring the absolute intensity of the beam as registered by the Beam Scintillator; the relative intensity of the Beam Scintillator versus the one given by the ionization chamber; the system dead time; the polarization of the beam as monitored by the SPES02π polarimeter, and resulted in the elimination of all abnormal beam bursts. The granularity of the SPES02π also permitted the use of the topology of events selected by the trigger to recognize and eliminate a significant amount of pollution coming from the beam halo as well as from p-p elastic scattering leaking through the anticoïncidence scintillators. Following this reduction of the data, cuts were made on the Beam Scintillator and lead-glass bars meantimer time spectra ensuring that the Beam Scintillator gave the start and thus eliminating most of the accidental coïncidences. These cuts reduced the total number of registered events by only 30% leaving a contamination of the order of 5% due to accidental coïncidences under the prompt peak. The large fraction ($\approx$ 50%) of good events filtered by the trigger demonstrates, a posteriori, the selectivity of the system resulting essentially from the good timing and the granularity of the SPES02π allowing an effective topological trigger.

Finally, the information given by the ADC was used to perform low energy cuts. The results of all the above treatments were controlled using two dimensional gamma energy spectra and the corresponding π^0 invariant mass. Fig. 2 shows such a two dimensional gamma energy spectrum corresponding to a final background to signal ratio of less than a few percent.

To derive physical observables from the data, one has to determine the efficiency of the system as accurately as possible. The efficiency depends on three main factors: *i)* the incident energy through the kinematics and the geometric acceptance of the detector, *ii)* the characteristics of the reaction, namely the π^0 angular distribution in the CM and the π^0 momentum distribution, and finally, *iii)* the photon detection efficiency in the lead-glass.

A Monto Carlo simulation program was written to take into account all those factors and the trigger configuration. The π^0 momenta, in the CM, were sorted according to either a statistical phase space distribution or a resonant phase space (the π^0 and the outgoing protons forming a Δ resonance). The real distribution lies somewhere between those two extremes [21,40]). The $pp \rightarrow pp\pi^0$ reaction is symmetric in the CM and the π^0 energy integrated angular distribution is usually represented by

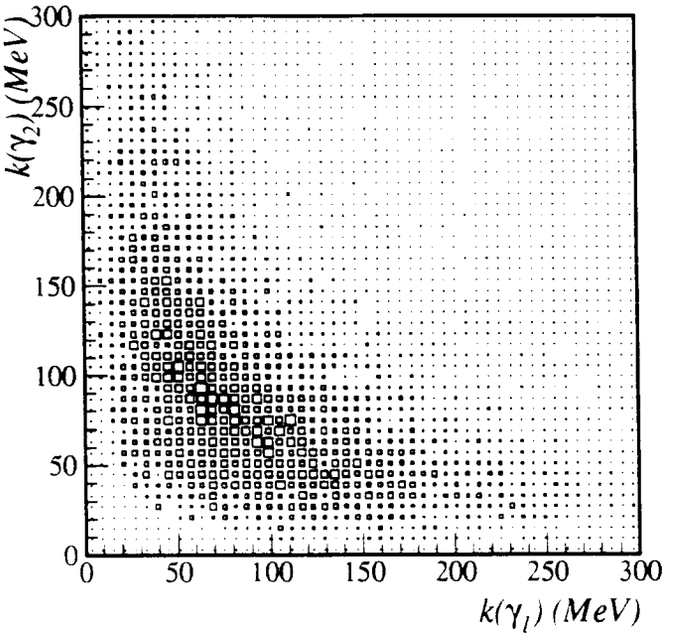

Fig. 2. Energy of the two photons after all cuts at an incident proton energy of 572 MeV.

the expression:

$$(d\sigma/d\Omega)_{CM} = K[\frac{1}{3} + b \cdot \cos^2(\Theta)] \tag{3.5}$$

where Θ in the π° CM angle and "b" is the anisotropy parameter, which has a value somewhere between 0 and 0.3. Again, we sort the initial π° according to either an isotropic distribution ($b = 0$) or an anisotropic one ($b = 0.3$). Having the π° vector momentum, one can calculate, by kinematical constraints, the vector of the associated "diproton" particle, and by sorting again, those corresponding to the two protons and the two decay photons of the final state. The impact pattern in the SPES02π provides the "geometrical" efficiency of the system. It depends, of course, on the initial assumptions concerning the phase space (Statistical or Resonant) and the angular distribution ($b = 0$ or $b = 0.3$), but has a predictable contribution on the accuracy of each observable measured in this work. We take it into account in the corresponding errors and we shall see, that the resulting uncertainty is smaller or at most comparable to those coming from other sources.

The determination of the photon detection efficiency in the lead-glass bars resulted from another simulation program based on the Electron Gamma Shower EGS program, developed at SLAC [36]). It furnished the values for the detection efficiency of one photon impinging on a lead-glass bar as a function of the photon energy and the impact position along the bar. This efficiency depends on an effective threshold expressed as a minimum number of Čerenkov photons produced in the glass [29]). This effective threshold was calibrated by measuring the efficiency of one section of the spectrometer in a tagged photon beam derived from the electron storage ring ELSA at the University of Bonn. These measured photon detection efficiencies as function of energy and impact position are in agreement with the simulation taking an effective threshold of 700 Čerenkov photons. [37,38]). Finally, the contribution coming from the target walls and the experimental hall never exceeded 25% of the full target contribution. It was subtracted from the main data using the production rates measured with an empty target.

3.2. TOTAL CROSS SECTIONS

Due to the 4π configuration of the SPES02π it is anticipated that total cross sections will not be strongly dependent on assumptions concerning the π° momentum and angular distributions. The simulation showed indeed that the global efficiency of our detector is insensitive to the π° CM angular distribution and that for the momentum distribution, the largest deviation from a mean value stayed well within $\pm 3\%$ at all incident energies. Therefore, we measured purposely the total cross sections at 325 MeV as a further check of the shower efficiency, since Meyer et al. [16]) have made this measurement near threshold, detecting the two outgoing protons in most of the phase space. It should be noted that those authors have no major detector efficiency problem, because they use scintillators. Furthermore, close to the

E_{beam} MeV	σ_T [μb]	b
325	8.1 ±0.5	0.08±0.11
460	271 ± 9	0.107±0.009
480	379 ± 8	0.120±0.011
500	542 ± 10	0.150±0.013
520	714 ± 13	0.265±0.018
540	959 ± 21	0.249±0.015
560	1235 ± 30	0.242±0.019
572	1413 ± 30	0.242±0.029
660	2807 ± 49	0.262±0.023
784	3806 ± 58	0.191±0.028
900	4535 ± 69	0.207±0.050
1012	4624 ± 70	0.26±0.19

TABLE 1

Total Cross Sections and Anisotropy factors of the $p(p,\pi^\circ)pp$ reaction.

threshold the production process cannot be resonant and its angular distribution is isotropic. This defines completely all the parameters of our simulation program at this energy. The agreement between their measurements and ours firmly established our effective threshold value for the shower efficiency parameter estimated previously rather empirically [6]).

Using the simulation program, we could calculate accurately the efficiency of the system. The global mean efficiency sinks from 16% at 325 MeV down to 6% at 1012 MeV. Using these efficiencies, we got the total cross sections displayed on fig. 3. The statistical uncertainties are negligible and the systematic error is less than 6%, coming essentially from the normalization procedure at 325 MeV and the uncertainty concerning the π° CM momentum distribution. Our points extend from 325 MeV until 1012 MeV and the corresponding numerical values are given in Table 1. Around 500 MeV incident energy, we used smaller energy steps (20 MeV) to investigate the region where a $T=1$, narrow dibaryon resonance was reported [39]). No indication can be seen in our excitation function. Between 572 MeV and 1012 MeV our points where chosen to fit the corresponding energies of the $np \rightarrow pp\pi^-$ of ref. [27]). Also displayed in fig. 3 are the results of previous experiments, the agreement among most of the points is remarkable in particular considering that some data have been taken more than 20 years ago.

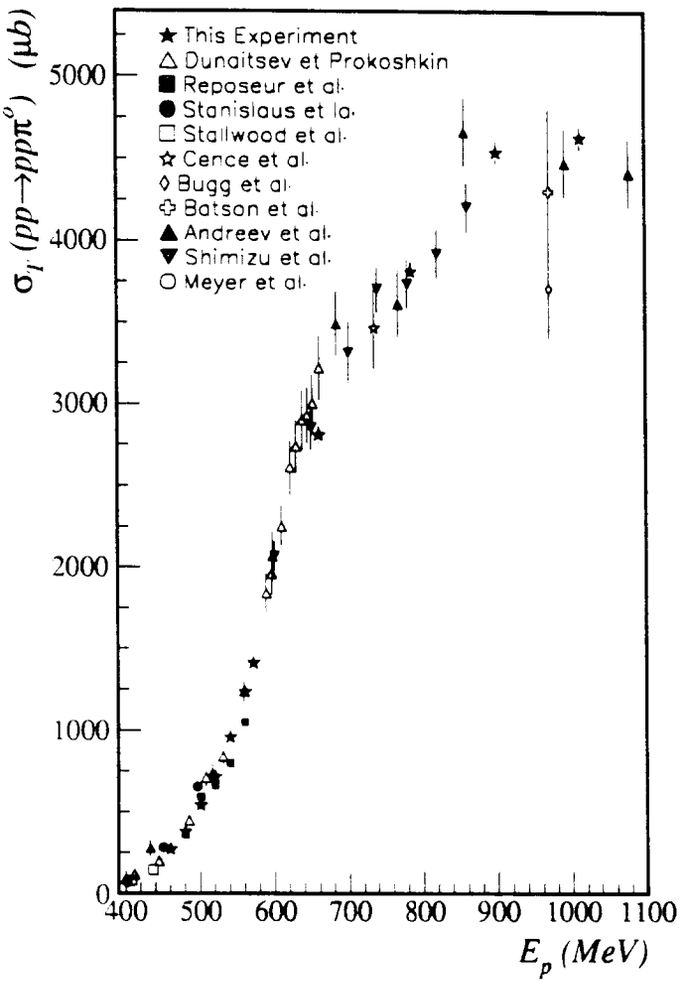

Fig. 3. Excitation function for the total cross sections of the $p(p, \pi^0)$ reaction.

3.3. ANGULAR DISTRIBUTIONS

Owing to the 4π configuration of the present detector, the anisotropy factor "b" given in relation in (3.5) could be measured directly for the first time. Simulation programs showed that the system is sensitive to the anisotropy of the π^0 energy integrated differential cross sections. In addition, the summation on π^0 energies in each CM angular bin reduces the influence of the rather poor energy resolution of the system precluding the precise determination of double differential cross sections. Using the simulation program, we calculated the angular efficiency as the ratio of the number of pions emitted at a given angle in the CM, divided by the number of pions effectively seen by the detector (fig.4). The ratio r (fig.4.3) served as a normalization factor for the measured rates (fig.4.1) in the corresponding angular bins. The product (fig.4.4) shows the real distribution of emitted pions and can be fitted with the function (3.5). As seen in fig. 1, the spectrometer does not cover forward angles smaller than 30 degrees. Therefore, the efficiency for π^0 emitted at forward angles gets smaller and smaller with increasing beam energy. The corresponding normalization factor r can reach values much larger than 10 (see fig. 4), thereby boosting any pollution occurring at forward angle, for example the charged particle leak mentioned earlier. We limited the angular distribution fit to the region with the ratio $r < 10$. Except for the two highest beam energies, the whole backward hemisphere in the CM corresponds to r values smaller than 10, making the fit meaningful, for a symmetric reaction as the one considered here.

The method to find the anisotropy factor is to reproduce the experimental angular distributions by sorting, in the simulation program, the initial π^0s according to relation (3.5). Since the normalization factor r depends on the initial choice of the anisotropy factor b, by feedback, it has a rather strong influence on the final fit: too small starting b resulted in the finding of too small anisotropy; and too big ones produced too big anisotropy. Ignoring the angular distribution which we want to measure, we always started two simulations with extreme initial anisotropies: b=0 and b=0.3, since b was always found, by other authors, smaller than 0.3. This first iteration produced two new "b" values which were entered as starting values into the next iteration. In all cases, three iterations were sufficient to ensure the convergence and reproduce safely the experimental distributions. This procedure had to be executed for the two typical π^0 momentum distributions corresponding to statistical and resonant phase space respectively. However, the averaging coming from the π^0 energy summation resulted in two fitted b values differing by less than 10% for the two π^0 momentum distributions considered. As final result, we kept the mean value and enlarged the error bars accordingly. The fits are shown in fig. 5, and the anisotropy factors are given in Table 1. Fig. 6 shows our results of the anisotropy factors as compared with those found by other authors. Our error bars are much smaller than those of any previous measurement for which the π^0 angular

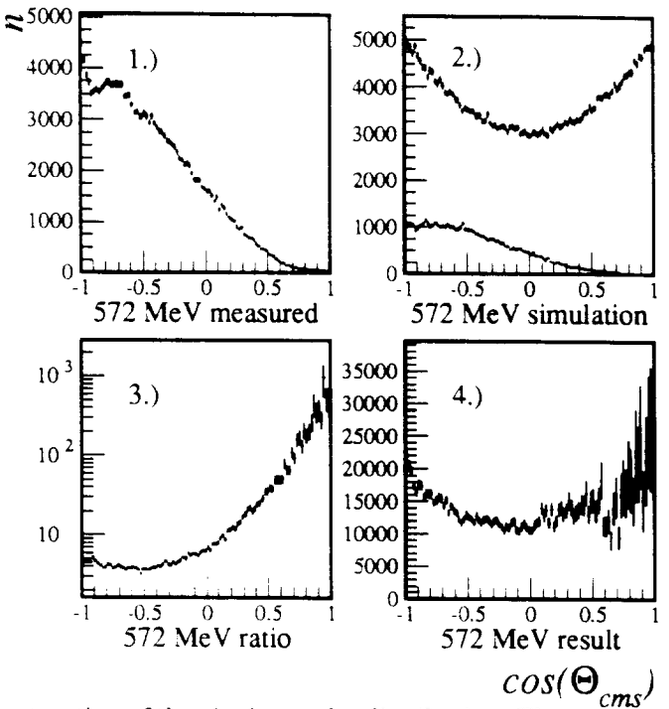

Fig. 4. Reconstruction of the pion's angular distribution. The measured distribution spectrum is shown in panel 1. The simulation distribution is the upper curve in panel 2, while the lower curve is the resulting pion's angular distribution from the simulated detector response. Panel 3 gives the ratio of panel 1 to the lower curve in panel 2. The final reconstructed angular distribution is given in panel 4.

distribution was not measured directly, either because the π° was not identified (one single γ detected [7,8,12]) or the two protons detected [15,40])) or the π° identified in a too small portion of the total phase space [10]).

The anisotropy factor increases gradually from $b = 0.1$ at 460 MeV to $b = 0.26$ at 520 MeV. That was not the case for the measurements of Dunaitsev and Prokoshkin [7]) and Stanislaus *et al.* [10]) who found very small anisotropies. But we confirm with more precise values those obtained by Cence *et al.* [12]) and Andreev *et al.* [15]) above 600 MeV.

Having the angular distribution for each beam energy, the total cross sections can be calculated from the differential cross section values as shown in fig. 5.

3.4. BEAM ASYMMETRY

The beam asymmetry A_y is defined by

$$A_y = \pm \frac{1}{p_{u,d}} \cdot \frac{L_{u,d} - q \cdot R_{u,d}}{L_{u,d} + q \cdot R_{u,d}} \qquad q = \frac{L_o}{R_o} \tag{3.6}$$

where the counting rates of π°s going to the left are defined by $(L_{u,d})$ and to the right by $(R_{u,d})$. The subscripts "u", "d" and "0", correspond to the beam polarization up, down and unpolarised respectively. The factor q takes into account the detector left right experimental bias and p is the beam polarisation. A_y is calculated, after summation on π° energies, for each angular bin and each polarization state of the proton beam. In order to have enough statistics we took 12 angular bins, 15^o wide each in the center of mass. We took only into account the π° emitted with a ϕ angle within $\pm$ 45 degrees from the horizontal reaction plan. The finite resolution and geometric acceptance of the detector could result in some distortion between the measured A_y and the physical one. As for the angular distributions, we have used a simulation program taking into account all the characteristics of the π° spectrometer to see how much the A_y could be attenuated by the experimental setup. As the average beam polarization was of the order of 85%, a simulated asymmetry of this polarization was generated using an angular distribution of the emitted π° in the "ϕ-plane" perpendicular to the beam, following a $1 + \cos(\phi)$ function for polarization "up" and $1 + \cos(\phi + \pi)$ for polarization "down". Then, the corresponding computer generated data were analyzed with the program used for the experimental data. The ratio between the resulting A_y and the input are shown in fig. 7 for four different beam energies spanning the energies measured here. For forward and backward angles, the attenuation is large, but moderate between 30 and 150 degree in the CM. The resultant experimental A_y are given in fig. 8; they are negative with a maximum of the order of -0.4 around 100 degrees CM. They were measured for the first time in such a large energy range. The already measured asymmetries for this reaction are those of Stanislaus *et al.* [10]) below 500

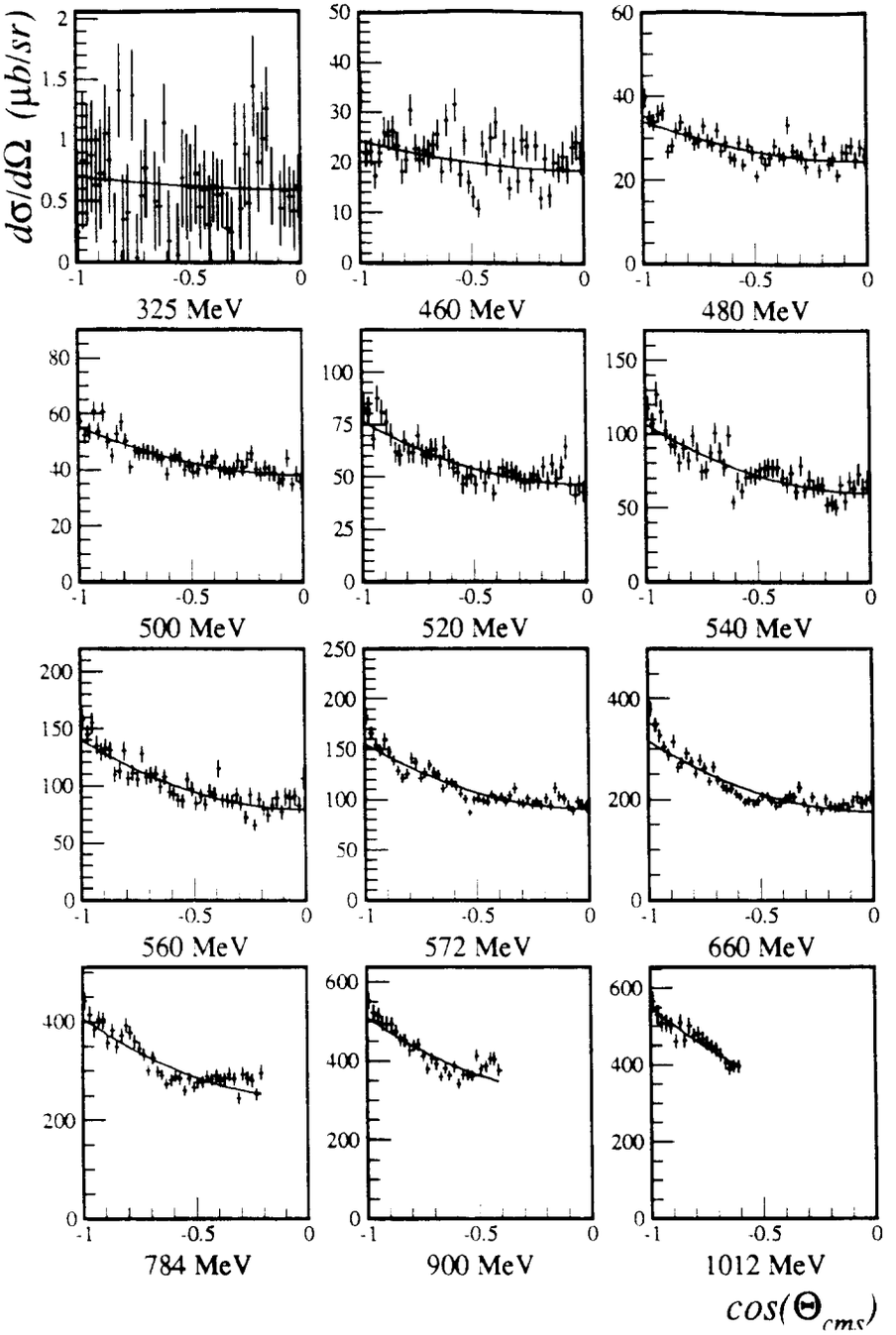

Fig. 5. Differential Cross Sections of the $p(p, \pi^0)pp$ reaction.

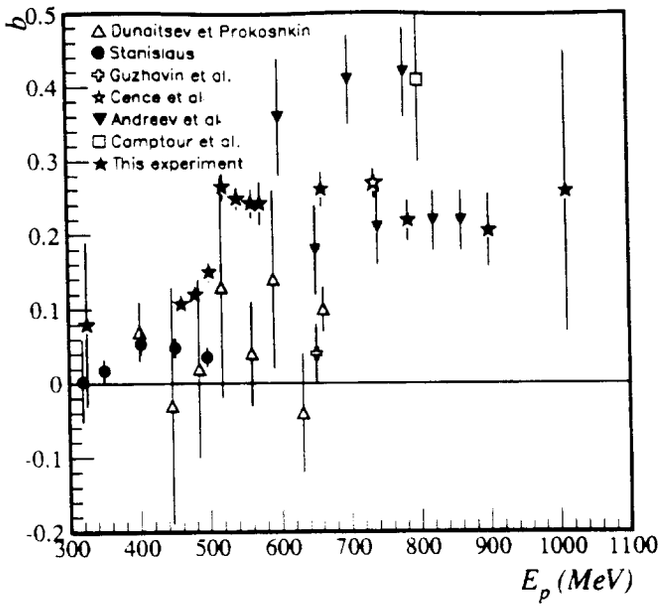

Fig. 6. Anisotropy factor b for the $p(p, \pi^0)pp$ reaction.

MeV they are negative with large error bars and compatible with our results. There is also one measurement at 800 MeV to be published [40]).

4. Discussion

Having now more data on reaction (1.1) and (1.2), we can attempt to derive more precisely the contribution of the nonresonant cross section σ_{01} than was done in the past [6,21]). Using relation (1.4), σ_{01} can be directly obtained from the total cross sections corresponding to the $\pi^{\pm}$ and π^0 channels respectively. However, care should be taken in choosing the corresponding incident energies for the proton and the neutron respectively, due to the mass differences between proton and neutron or $\pi^{\pm}$ and π^0. One can consider to subtract the total cross sections at incident energies corresponding to the same center of mass energy "$\sqrt{s}$" in both channels which emphasizes the role of the initial state

$$s = (P_1 + P_2)^2 = m_1^2 + m_2^2 + 2(E_1 + m_1)m_2, \tag{4.7}$$

or the same maximum momentum for the π emitted in the final state

$$\eta_m = \frac{\sqrt{(s - m_3^2 - (m_4 + m_5)^2)^2 - 4m_3^2(m_4 + m_5)^2}}{2m_3\sqrt{s}}, \tag{4.8}$$

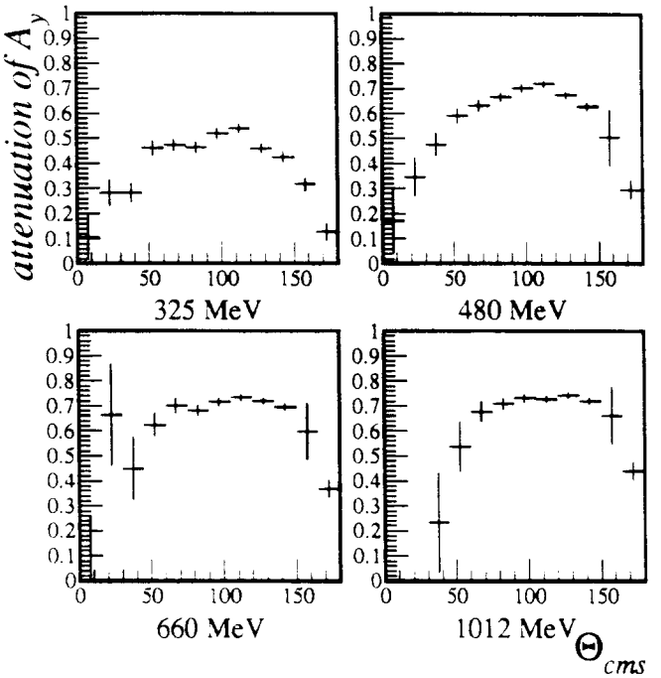

Fig. 7. Simulated attenuation of beam asymmetry A_y for four different beam energies.

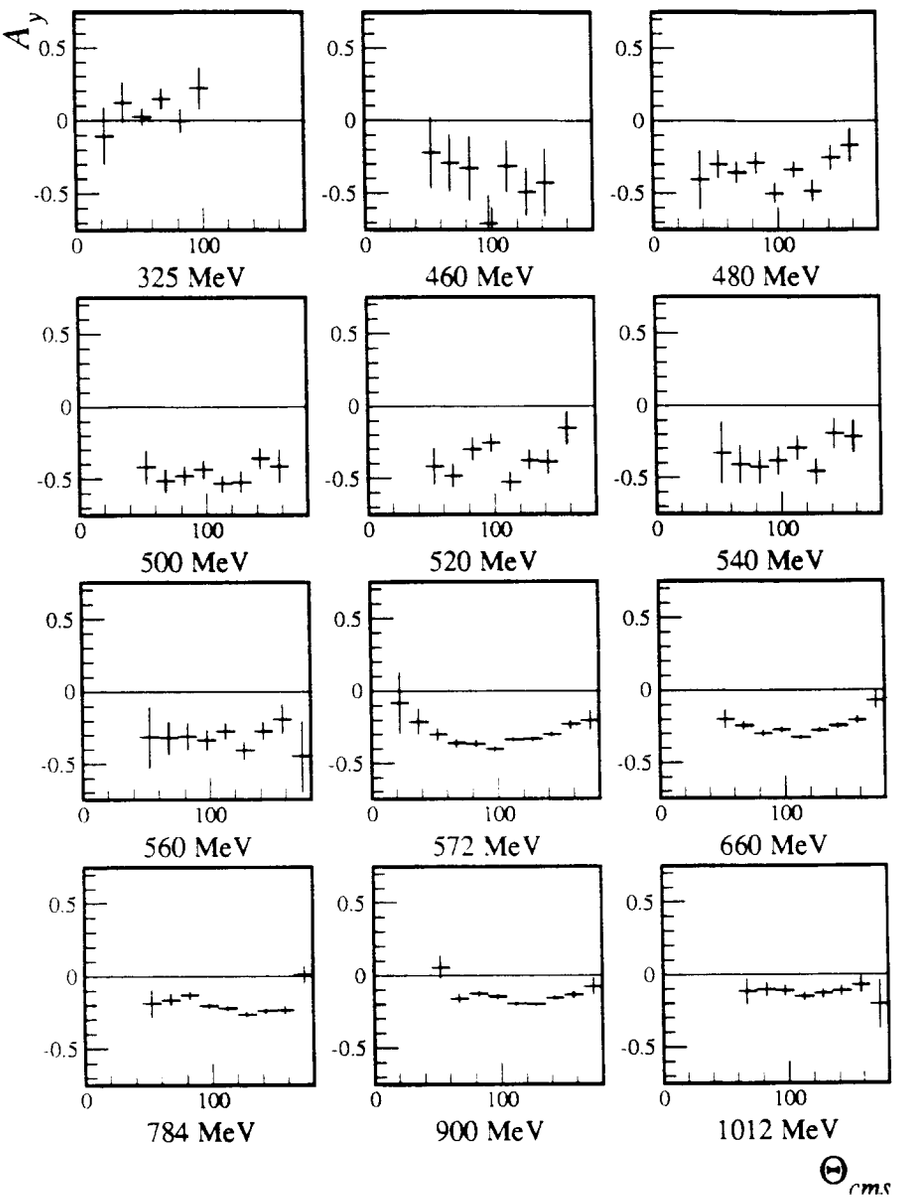

Fig. 8. Beam Asymmetry A_y for the $p(p, \pi^0)pp$ reaction.

where the m_3 is the pion's mass and $m_{4,5}$ the outgoing nucleon's masses. For a given proton energy, the "η_m" prescription gives neutron energies higher by 11 to 37 MeV in our energy range, while for the "$\sqrt{s}$" prescription, corresponding neutron energies will be 2.6 MeV lower. Due to the fast rise of σ_T as a function of incident energy, the two prescriptions will give very different results as can be seen in fig. 9. For the neutron data we have used published values [18-25]) as shown in fig. 10 and attempted a polynomial fit to get the excitation function at any neutron energy. However, below 600 MeV incident energy, the neutron data slope is governed by the results of the Freiburg group [21,25]) and above by those of Ref. [24]). The incompatibility between those two slopes around 600 MeV generates the discontinuity observed for σ_{01} around this energy. However, the rise of σ_{01} above 600 MeV is consistent with the predictions of VerWest and Arndt [1]) from their phase shift analysis and is expected due to the onset of the N^* resonances. Below 600 MeV we confirm the results for σ_{01} obtained in [21]) although they used less precise values of σ_{11}.

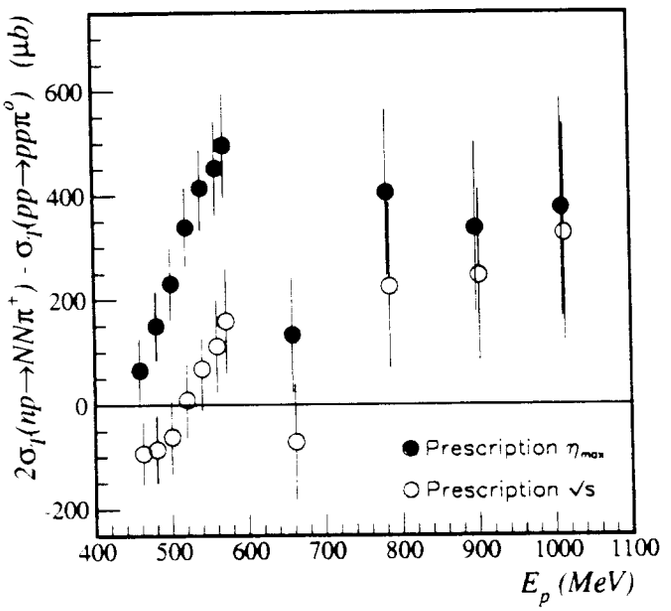

Fig. 9. Partial Cross Section σ_{01} calculated from our results for the reaction $pp\rightarrow pp\pi^o$ and literature values for the reactions $np\rightarrow NN\pi^{\pm}$.

In this energy region, the recent data of ref. [26]) concerning the angular distributions of reaction (1.2) allows interesting considerations. Fig. 11 shows a comparison of the anisotropy factor "b" for reactions (1.1) and (1.2). The π^o have a moderate

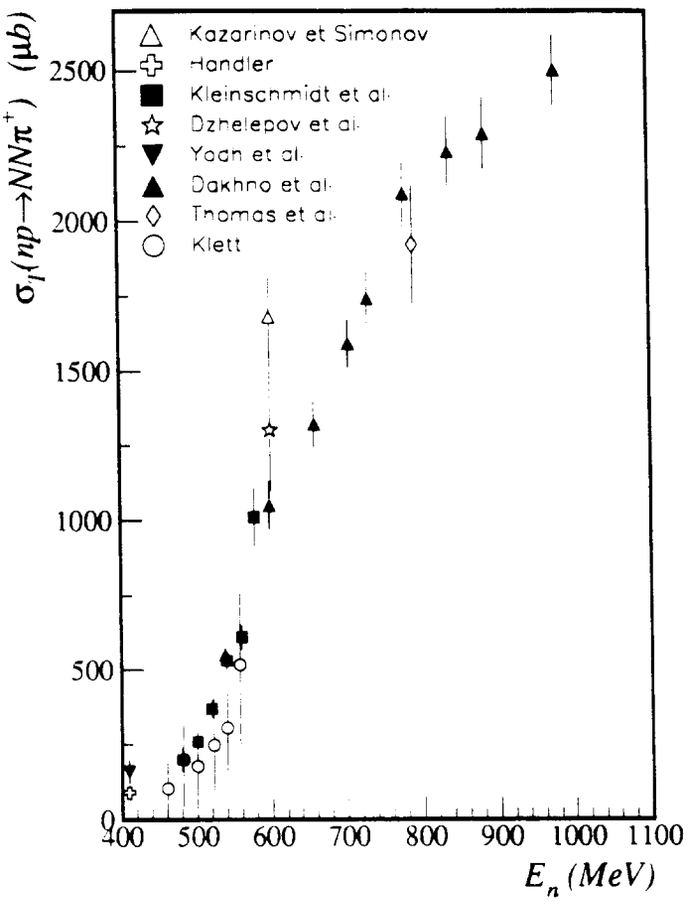

Fig. 10. Total Cross section data of the reaction $np \rightarrow NN\pi^{\pm}$.

anisotropy through the whole energy range, while the $\pi^{\pm}$, although comparable to the π° near threshold and above 600 MeV show a stronger anisotropy, peaking around 540 MeV. It should be noted that the observed difference is much larger than the experimental errors on our π° experiment and on the recent Bannwarth results for the $\pi^{\pm}$. Our present results, for reaction (1.1) confirm with a better precision those published previous by [7,8,10,12,15]). In the same way, for reaction (1.2), the values of Bannwarth et al. [26]) are of very good quality and consistent with the less precise previous ones [21]); in addition, they have measured a sizable $\cos(\Theta)$ term (dissymmetry) in the charged pions angular distribution by looking simultaneously at the outgoing π^{+} and π^{-}. So, the difference in the angular distributions corresponding to reaction (1.1) and (1.2) is a general feature of all data, but is now firmly established by the recent high quality data.

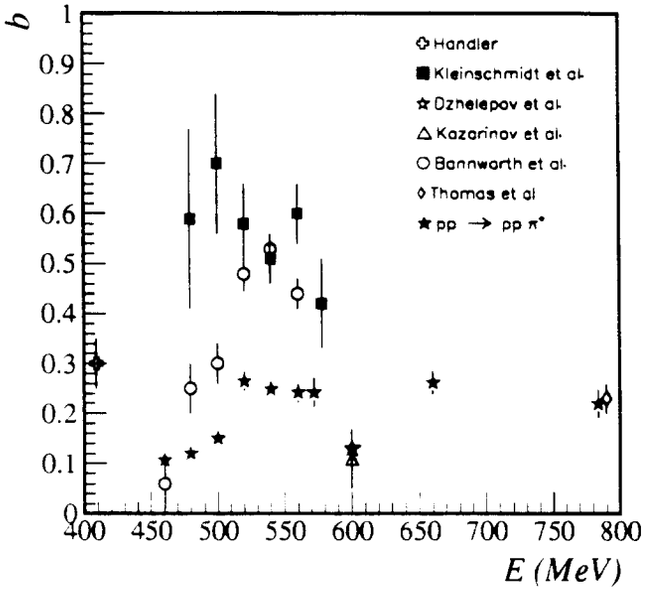

Fig. 11. Anisotropy factor b values previously reported for the reaction np$\rightarrow$NN$\pi^{\pm}$ as compared to the values reported here for the reaction $p(p, \pi^{\circ})pp$.

It has been suggested [26]) that a sizable σ_{01} contribution from the $^3D_1$ partial wave could be responsible for this effect. To get quantitative estimates, we have attempted a partial wave fit of the data at 480, 540, and 600 MeV assuming that in this energy range a limited number of partial waves would contribute. The method consists in fitting our $pp\pi^{\circ}$ observables with the minimum number of transitions to fix the "σ_{11}" contribution common to reaction (1.1) and (1.2). Then to fix the additional "σ_{01}" contribution by fitting the $\pi^{\pm}$ anisotropy and dissymmetry

	Transition	480 MeV	540 MeV	600 MeV
$T_i = 0$	$^3S_1 \rightarrow {}^1S_0p_1$	0.5	0.6	0.6
	$^3D_1 \rightarrow {}^1S_0p_1$	1.0	2.8	1.38
	$^1F_3 \rightarrow {}^3P_2p_3$	0.05	0.055	0.35
$T_i = 1$	$^3P_0 \rightarrow {}^1S_0s_0$	1.2	1.86	2.4
	$^1D_2 \rightarrow {}^3P_2s_2$	0.89	0.93	1.4
	$^3F_3 \rightarrow {}^3P_2p_3$	0.55	1.14	1.75

TABLE 2

Amplitudes for the six transitions taken into account to reproduce the inelastic cross sections.

given in ref. [26]). Considering in the final state, only S and P waves for the NN system and the π relative to NN, one gets twelve σ_{11} transitions and nine σ_{01} ones. The selection of particular transitions is based on quantitative arguments given in detail in ref. [41]). Final states with the two nucleons in a $^1S_0$ configuration have been retained systematically because of their importance in the low energy NN scattering. The need for positive "b" values (anisotropy) and negative beam asymmetries peaking around 90° CM, has mainly motivated the choice of the other 3 transitions. In particular the $^3F_3 \rightarrow {}^3P_2p_3$ transition gives rise to a diagonal term having the largest contribution to the π^0 anisotropy and requires the $^1D_2 \rightarrow {}^3P_2s_2$ for a large contribution to the asymmetry by interference. Although our final choice is not unique it stayed fairly stable when other transitions were added, even the $^1F_3 \rightarrow {}^3P_2p_3$ transition could be left out and is only there to adjust the "$\cos\Theta$" term measured in reference [26]). Table 2 gives the amplitudes of the transitions fitted at 3 different energies and the quality of the fit can be appreciated from Table 3, where the mean values of experimental parameters are compared to the calculated ones. It is remarkable, from table 2, that the isoscalar initial state is completely dominated by the $^3D_1$ partial wave which has a resonant behavior centered around 540 MeV.

In the partial wave approach described here, we have considered that anisotropy factors are now much more reliably known in the energy range 400-500 MeV than absolute values of the cross sections. Such is not the case at higher energy where measurements for reaction (1.2) are old and sparse, but the few existing results are consistent with similar anisotropies for reaction (1.1) and (1.2). Accordingly, the partial wave analysis performed here indicates a significant contribution due to σ_{01}, below 600 MeV and peaking around 540 MeV. It is a pity that recent investigations of reaction (1.2) [27,28]) have been limited to polarisation observable measurements and have not extracted from the data neither the angular distributions nor the total cross sections.

One of the goals of the present experimental investigation was to search around 520 MeV, for a possible indication in the total cross section due to a narrow isovector

E_i	480 MeV	540 MeV	600 MeV
	π^0 $\pi^\pm$	π^0 $\pi^\pm$	π^0 $\pi^\pm$
$\sigma_T(\mu b)$	380 240	960 850	2100 1200
K^{exp}	81 46	184 133	398 227
K^{th}	82 48	187 138	410 226
b^{exp}	0.12 0.25	0.249 0.53	0.26 0.26
b^{th}	0.13 0.226	0.242 0.49	0.26 0.27
a_1^{exp}	0 $\mp$5.	0 $\mp$7.5	0
a_1^{th}	0 $\mp$4.8	0 $\mp$7.6	0 $\pm$2.5

TABLE 3

Comparison between calculated (th) and measured (exp) parameters for the cross sections. K and b are defined by equation the (3.5); a_1 is the $\cos(\Theta)$ coefficient when one expresses the cross section by $(d\sigma/d\Omega) = a_o + a_1 \cdot \cos(\Theta) + a_2 \cdot \cos^2(\Theta)$.

dibaryon [39]). In this region, σ_T is perfectly smooth, in spite of our efforts to scan the region by small energy steps (20 MeV). However, it is amazing, that we find in the same energy region a strong indication for a localized contribution in the isoscalar channel.

In principle, one could also get information on the difference between neutral and charged pion channels by comparing the corresponding asymmetries. Here, we benefit from the recent kinematically complete data of ref. [27,28]) and we have purposely chosen our high energy points to match those of ref. [27]). We have measured beam asymmetries for π^0 emitted at a given angle in the CM by summing on all π^0 energies. As in ref. [27]) we find negative asymmetries with a maximum value of -0.4 around 100° CM (see fig. 8), however, at small angles we never get to small positive values as in ref. [27]). It is difficult to exploit simply the asymmetry data; in fact, our partial wave fit shows that, in both cases, for reaction (1.1) and (1.2), all partial waves contribute.

It is also a challenge for phenomenological models to reproduce, even the sign of our measured asymmetries. As in ref. [6]), we use the peripheral model of Laget to reproduce our data on a much wider energy range than before. A detailed description of the model can be found in ref. [6]) and references therein. The results are shown in fig. 12 for the total cross sections and in fig. 13 for the anisotropy parameters. The predictions are very good for σ_T, fair for "b", but have the wrong sign for the "A_y". The inclusion of N-Δ rescattering (as in the $\gamma D \rightarrow pp\pi^-$ reaction) [42]) does not change this picture: while it modifies the total cross sections at the level of 20% it does not help to change the sign of the polarization. Pion rescattering,

which is not yet included in this model, may cure the problem.

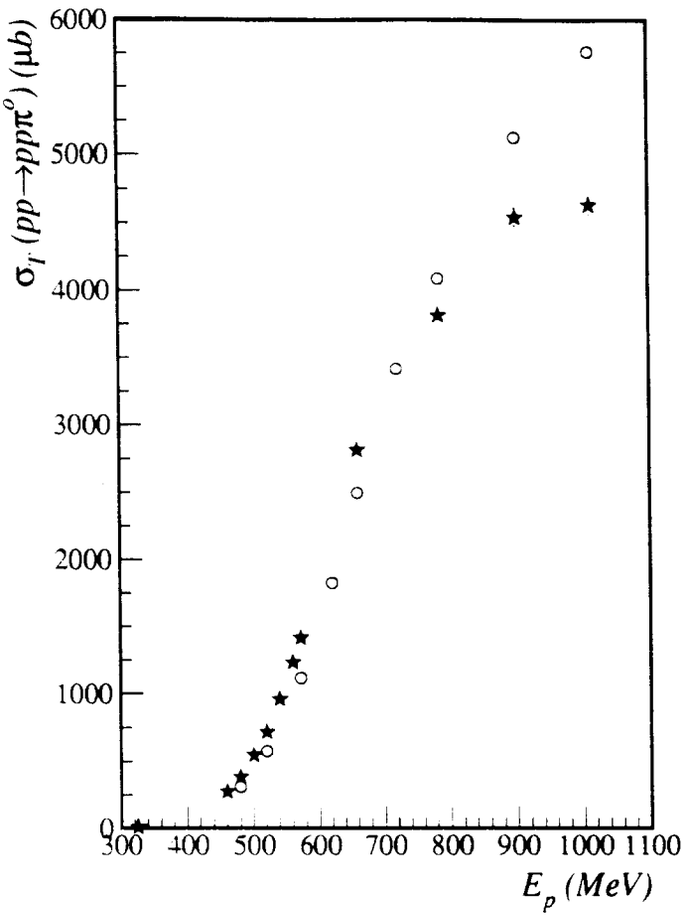

Fig. 12. Comparisons of the measured total cross section of the reaction $p(p,\pi^0)pp$ (solid stars) to peripheral model of Laget (open circles).

5. Conclusions

We have used a fairly simple π^0 spectrometer in a 4π configuration to measure the total cross sections, the angular distributions and the beam asymmetries for the reaction $p(p,\pi^0)pp$ from threshold to 1 GeV. A complete and detailed simulation of the response of the detector and calibration of its efficiency allowed the measure of those observables with a much higher accuracy than ever before. In particular, angular distributions have been measured directly for the first time, looking at the

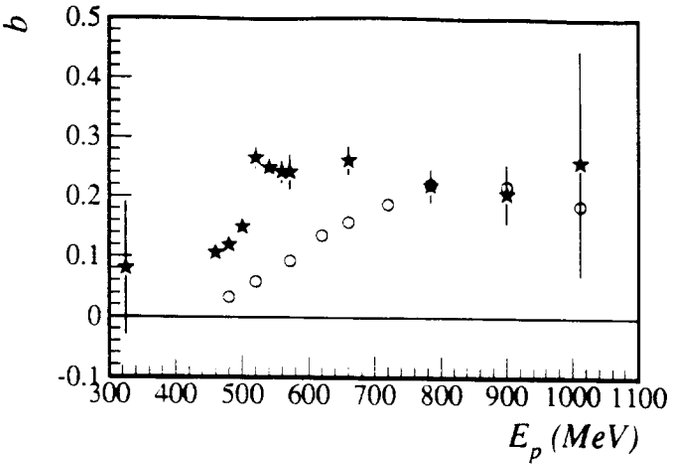

Fig. 13. Comparisons of the measured anisotropic parameters of the reaction $p(p,\pi^\circ)pp$ (solid stars) to the peripheral model of Laget (open circles).

outgoing π°. Also, most of the asymmetry data are new.

We do not see in σ_T any enhancement due to a possible isovector dibaryon reported around 520 MeV. Assuming charge invariance, the comparison with the $np \rightarrow NN\pi^\pm$ reactions allowed us to derive, from the total cross section significant non resonant σ_{01} cross section increasing above 600 MeV with incident energy as expected from the onset of N^* resonances. The most interesting result of the present experimental investigation is the large difference between the angular distribution corresponding to π° and $\pi^\pm$ production, appearing below the Δ resonance region (600 MeV). We derive through a partial wave fit a localized σ_{01} contribution peaking at 540 MeV, dominated by the $^3D_1$ wave in the initial isoscalar channel. Finally, our fairly complete set of data for one of the most elementary hadronic π° production reactions, involving only $T=1$ nucleon states, provides a good test for phenomenological models, and in particular, the negative beam asymmetries which are difficult to reproduce.

References

1) B.J. VerWest and R.A. Arndt, Phys. Rev.**C25** (1982) 1979
2) J. Bystricky *et al.*, J. Physique **48** (1987) 199
3) H. Garcilazo and T. Mizutani, πNN Systems (World Scientific, Singapore, 1990)
4) A.H. Rosenfeld, Phys. Rev. **96** (1954) 139
5) M. Gell-Mann and K.M. Watson, Ann. Rev. Nucl. SC.4 (1954) 219
6) J.P. Didelez *et al.* Nucl. Phys. **A535** (1991) 445
7) A.F. Dunaitsev and Y.D. Prokoshkin, Sov. Phys. JETP **9** (1959) 1179
8) A.F. Dunaitsev and Y.D. Prokoshkin, Sov. Phys. JETP 11 (1960) 540

9) T. Reposeur, Thèse de Doctorat, d'Université Paris VII, IPNO-T-89-05 (1989)
10) S. Stanislaus *et al.*, Phys. Rev. **C44** (1991) 2287
11) R.A. Stallwood *et al.*, Phys. Rev. **109** (1958) 1716
12) R.J. Cence *et al.*, Phys. Rev. **131** (1963) 2713
13) D.V. Bugg *et al.*, Phys. Rev. **C41** (1990) 2708
14) A.P. Batson *et al.*, Proc. Roy. Soc. **A251** (1959) 233
15) V.P. Andreev *et al.*, Z. Phys. **A329** (1988) 371
16) H.O. Meyer *et al.*, Phys. Rev. Lett. **65** (1990) 2846
17) F. Shimizu *et al.*, Nucl. Phys. **A389** (1982) 445
18) G.B. Yodh, Phys. Rev. **98** (1955) 1330
19) R. Handler, Phys. Rev. **138** (1965) B1230
20) V.P. Dzehelpov *et al.*, JETP **50** (1966) 993
21) M. Kleinschmidt *et al.*, Z.Physik **A298** (1980) 253
22) Yu.M. Kazarinov and Yu.N. Simonov, Sov.Jour.Nucl.Phys. **4** (1967) 100
23) W. Thomas *et al.*, Phys. Rev. **D24** (1981) 1736
24) L.G. Dakhno *et al.*, Phys. Lett. **B114** (1982) 409
25) A. Klett, Doktorarbeit, Universität Freiburg, Germany, unpublished, (1987)
26) Bannwarth *et al.*, Nucl. Phys. **A507** (1994) 761
27) Y. Terrien, *et al.*, Phys. Lett. **B294** (1992) 40
28) M.G. Bachman, PhD Thesis, University of Texas at Austin, unpublished, (1993) see also M.G. Bachman *et al.* FewBody XIV, Amsterdam 1993, ed. B.L.G. Bakker and R. van Dantzig in Few Body Systems, supplementum 7 (Springer-Verlag, 1994) p.225
29) M. Rigney, PhD Thesis, University of South Carolina, unpublished (1992).
G. Rappenecker, "Thèse d'Université" Orsay(1992), Int. Rep. IPNO-T. 92-05
30) Schott-Mainz, Reference catalogue, F2 glass: n=1.62 at λ=5876 Å; n=1.65 at λ=4047 Å. X_0=3.3 cm, $\rho = 3.61\ g/cm^3$.
31) Philips Compenents, Photomultiplier Data Handbook, pc04 (1990).
32) G. Battistoni *et al.*, Nucl. Instr. Meth. **164** (1979) 57
33) Manuel des Utilisateurs de Saturne, LNS, Saclay (1991).
34) C. P. Anderson, " Introduction to Q", Los Alamos National Laboratory report MP-1-3401-3 (1985)
35) Model 2372, Memory Lookup Unit Technical Description, by LeCroy Research Systems Corporation, Spring Valley, New York 10977.
36) R. Ford and W. R. Nelson, "The EGS4 Code system", Stanford Linear Accelerator Center report SLAC-265 (1985)
37) M. Rigney *et al.* to be submitted to NIM
38) M. Mayers, Masters Thesis, University of South Carolina, unpublished (1993)
39) B. Tatischeff *et al.*, Phys. Rev. **C36** (1987) 1995
40) C. Comptour *et al.*, Internal Report, DAPNIA/SPhN 9405 CEA Saclay, (1994)
41) J. Van de Wiele, "Multipole Anaylysis of the $N+N \rightarrow N+N+\pi$ Amplitudes: Formalisms.", Internal Report IPNO-dre 95-06. Institut de Physique Nucléaire, Orsay (1995).
42) J.M. Laget *et al.*, Phys. Rep. **G9** (1981) 1